HHS Public Access

Author manuscript

Strahlenther Onkol. Author manuscript; available in PMC 2020 February 01.

Published in final edited form as:

Strahlenther Onkol. 2019 February ; 195(2): 121–130. doi:10.1007/s00066-018-1348-5.

Towards Universal MRI Atlas of the Prostate and Prostate Zones: Evaluation of Performance between Vendor and Acquisition Parameters

Kyle R. Padgett, Ph.D.[1,2], **Amy Swallen, B.S.**[3], **Sara Pirozzi, B.S.**[3], **Jon Piper, B.S.**[3], **Felix M. Chinea, M.D.**[1], **Matthew C. Abramowitz, M.D.**[1], **Aaron Nelson, M.D.**[3], **Alan Pollack, M.D., Ph.D.**[1], and **Radka Stoyanova, Ph.D.**[1,*]

[1]Department of Radiation Oncology, University of Miami Miller School of Medicine, Miami, FL, USA; [2]Department of Radiology, University of Miami Miller School of Medicine, Miami, FL, USA; [3]Research and Development, MIM software Inc., Cleveland, OH.

Abstract

Background and Purpose—To evaluate an automatic multi-atlas-based segmentation method for generating prostate, peripheral and transition zone (PZ/TZ) contours on MRIs with and without fat-saturation (+/−FS), and MRIs from different vendor MRI systems.

Methods—T2-weighted (T2) and Fat Saturated (T2FS) MRIs were acquired on 3T GE and Siemens systems. Manual prostate and PZ contours were used to create atlas libraries. As a test-MRI is entered, the procedure for atlas segmentation automatically identifies the atlas subjects that best match the test subject, followed by a normalized intensity-based free-form deformable registration. The contours are transformed to the test subject and Dice Similarity Coefficients (DSC) and Hausdorff distance between atlas-generated and manual contours were used to assess performance.

Results—Three atlases were generated based on GE_T2 (n=30), GE_T2FS (n=30), and Siem_T2FS (n=31). When test images matched the contrast and vendor of the atlas, DSCs of 81 and 0.83 for T2+/−FS were obtained (baseline performance). Atlases performed with higher accuracy when segmenting: ***(i)*** T2FS vs T2 images, likely due to a superior contrast between prostate vs surrounding tissue; ***(ii)*** prostate vs zonal anatomy; (iii) in the mid gland vs base and apex. Atlases performance declined when tested with images with differing contrast and MRI vendor. Conversely, combined atlases showed similar performance to baseline.

Conclusion—The MRI atlas-based segmentation method achieved good results for prostate, PZ and TZ compared to expert contoured volumes. Combined atlases performed similarly to matching atlas and scan type. The technique is fast, fully automatic and implemented on commercially available clinical platform.

[*]Corresponding author: Radka Stoyanova, Ph.D. Department of Radiation Oncology University of Miami Miller School of Medicine 1475 NW 12th Avenue, Suite 1515J Miami, Florida 33136, USA Phone: (305)-243-5856, RStoyanova@med.miami.edu.

Conflict of Interest:

A.S., S.P., J.P., A.N., were employed by MIM Software Inc. during the duration of this investigation. Additionally, J.P. and A.N. have an ownership interest in MIM Software Inc. K.P., F.C., M.A., A.P. and R.S. have no conflicts of interest to disclose.

Abstract

Beurteilung einer automatischen Multi-Atlas-basiereden Segmentierungsmethode zur Erzeugung von Prostata-, Peripheren und LJbergangszonenkonturen (PZ/TZ) auf MRT Bildern (MRTs) mit und ohne Fettsattigung (+/− FS) und von MRT-Systemen verschiedener Hersteller.

T2-gewichtete (T2) und fettgesattigte (T2FS) MRTs wurden auf 3T GE- und Siemens-Systemen aufgenommen. Manuelle Prostata- und PZ-Konturen wurden verwendet, um Atlas-Bibliotheken zu erstellen. Nach dem Einlesen eines MRT Testdatensatzes, identifiziert das Verfahren zur Atlassegmentierung automatisch die Atlasobjekte, die am besten zum Testobjekt passen, gefolgt von einer normalisierten, intensitatsbasierenden, frei deformierbaren Registrierung. Die Konturen werden dem Testobjekt angepasst, und die ‘Dice Similarity Coefficients’ (DSC) und Hausdorff-Abstand zwischen atlasgenerierten und manuellen Konturen verwendet, um die LJbereinstimmung zu beurteilen.

Drei Atlanten wurden basierend auf GE T2 (n = 30), GE T2FS (n = 30) und Siem_T2FS (n = 31) erstellt. Wenn die Testbilder mit dem gewahlten Kontrast und Atlashersteller ubereinstimmten, wurden DSC von 0,81 und 0,83 fur T2 +/− FS erhalten (Ausgangswert). Atlanten erreichten eine hohere Genauigkeit beim Segmentieren von: (***(i)***) T2FS Bildern verglichen mit T2 Bildern, wahrscheinlich aufgrund des besseren Kontrastes zwischen Prostata und umgebenden Gewebe auf T2FS Bildern; ***(ii)*** Prostata verglichen mit zonaler Anatomie;***(iii)*** der Drüsenmitte verglichen mit Basis und Apex. Die Qualität der Atlanten ging zurück, wenn sie mit Bildern mit unterschiedlichem Kontrast und MRT-Gerät getestet wurden. Umgekehrt zeigten kombinierte Atlanten eine ähnliche Übereinstimmung und Qualität wie der Ausgangswert.

Die MRT-Atlas-basierende Segmentierungsmethode erzielte gute Ergebnisse fur Prostata, PZ und TZ im Vergleich zu konturierten Volumina. Kombinierte Atlanten erreichten eine ahnliche LJbereinstimmung und Genauigkeit wie passender Atlas und Scan-Typ. Die Technik ist schnell, vollautomatisch und auf einer kommerziell erhaltlichen klinischen Plattform implementiert.

Keywords

prostate; prostate zones; segmentation; MRI

INTRODUCTION:

Accurate prostate segmentation on MRI datasets is required for many clinical and research applications including diagnosis, staging, and treatment planning for prostate cancer. The prostate has two distinct regions, observable on imaging - the peripheral zone (PZ), characterized with high signal on T2-weighted MRI and transition zone (TZ), that appears darker than the PZ on T2. T2 contrast in the prostate reflects the different amounts of macromolecular and free water present: the PZ is composed of highly glandular-ductal tissues appearing bright on T2, while the TZ, composed of more stromal than ductal tissues, appears hypointense. The different imaging properties of the prostate zones are well recognized and reflected in the recommendations of the European Society of Urogenital Radiology (ESUR) guidelines for Prostate Imaging, Reporting and Diagnosis System

(PIRADS) [1,2] Prostate cancer identification and staging on MRI rely on accurate zonal classification.

Automatic segmentation of the prostate, PZ and TZ on MR images provides an opportunity to broaden the current scope of research by facilitating studies that include large populations of subjects and/or studies that incorporate serial imaging of the prostate to provide a longitudinal picture of disease progression and response. This is of a paramount importance for the application of high-throughput approaches for extraction of radiomics features [3]. Manual segmentation is not feasible as it is time consuming. The prostate and zonal contours are necessary for the identification of the dominant lesions on MRI that will allow for precise targeting of MRI-Ultrasound fusion (MRI-US) targeted biopsies [4–6] and delivery of a targeted radiation boost or other focal treatments to the designated area [7‘8]. Another potential application includes precise contouring of radiation targets for treatment planning, which is necessary for both intensity modulated radiotherapy (IMRT) and volumetric arc therapy treatment techniques and critical in hypofractionated radiotherapy of the prostate where large daily radiation doses are utilized, automatic segmentation may aid in these efforts[9]. Additionally, with MRI guided adaptive radiation treatments now a possibility with systems like Viewray and Elekta, automatic segmentation techniques are a key component of an efficient adaptive treatment planning program [10], other adaptive treatment planning applications, such as adaptive planning for intensity-modulated particle therapy, could also significantly benefit from automatic prostate segmentation[11].

Due to this increased role of MRI in prostate cancer diagnosis, treatment and research,prostate MRI image segmentation has been an area of intense research [12]. The Prostate MR Image Segmentation (PROMISE12) challenge aimed to standardize evaluation and objectively compare algorithm performance of the segmentation of prostate MRI. Several promising automatic, semi-automatic and interactive approaches were evaluated,[12] including atlas-based segmentation techniques [13–15]. Because of the excellent depiction of the prostate and surrounding anatomy, the high signal-to-noise ratio (SNR), and high spatial resolution, [12,16,17] T2-weighted MRI is the sequence of choice for building a prostate atlas[12,18–22]. More recently, several studies[2123–25] provide also segmentation of the prostate zonal structures [21,23–25]The presented approaches vary from model-based[26,27], to atlas-based segmentation[15,18–21,28]

The goal of this work is to implement a robust procedure for prostate and prostate zones segmentation in a clinical imaging platform MIM (MIM Software Inc, Cleveland, OH, USA). State of the art techniques are streamlined through an efficient implementation of multi-atlas- based segmentation. Most of prostate segmentation developments are carried out in custom platforms/software and are inaccessible to clinicians and researchers. With the objective of creating broad access to automatic segmentation, the performance of the atlas approach is evaluated, using ***(i)*** T2-weighted sequences, with and without fat-saturation (+/−FS), and ***(ii)*** data form different MRI manufacturers. An universal MIM atlas that is able to segment the prostate and prostate zones, regardless of acquisition protocols, magnetic field strength or type of scanners, will allow unprecedented access to clinicians and researchers.

METHODS

Study Cohort and MRI Acquisition:

An Institutional Review Board (IRB) approved a protocol titled "Development of Methods for Analysis and Interpretation of in vivo Imaging of Prostate Cancer" for retrospective review of MRI exams from patients with biopsy proven prostate cancer, protocol #20090554. A total of 30 consecutive patients, evaluated for radiation treatment from May 2012 through November 2013 scanned on a Discovery MR750 3T MRI (GE, Waukesha, WI, USA) and 31 patients scanned from December 2008 through January 2014 on a Magnetom 3T Trio (Siemens, Erlangen, Germany) were utilized. Patients' clinical characteristics are summarized in Supporting Table S1

Transverse T2-weighted MRI, acquired on GE with (T2FS) and without (T2) fat saturation, were at identical spatial resolution: $0.7\times0.7\times2.5\ mm^3$, 72 axial slices, no gap. Only T2FS sequence was analyzed for Siemens. Imaging of the pelvis was acquired with parameters (Table 1) based on recommended specification for clinical applications of prostate MRI[29].

Study Design:

The goal of the study was to determine the performance of atlas segmentation methods for delineation of the prostate and prostate zones (PZ and TZ). The central zone is not treated separately from TZ in this analysis because it is difficult to differentiate from TZ [30]. An analysis schema is presented on Figure 1. The three types of data are; GE T2, GE T2FS, and Siem_T2FS. Correspondingly, three atlases were generated: aGE_T2 (30 subjects), aGE_T2FS (30 subjects), and aSiem_T2FS (31 subjects), based on manually contoured prostate and PZ by an expert radiation oncologist, 26 years of experience. In addition, two combined atlases were created: aContrast(combined) = aGE_T2 U aGE_T2FS (60 subjects) and aVendor(combined) = aGE_T2FS U aSiem_T2FS (61 subjects). The five atlases are schematically presented in Figure 1. The performance of all atlases are evaluated using both the Dice Similarity Coefficient (DSC) [31] and Hausdorff distance metrics [32] The DSC value is a simple and useful summary measure of spatial overlap, which is often applied to measure accuracy and reproducibility of image segmentation,[33] DSC values are calculated using the equation shown below. The Hausdorff distance represents a measure of the spatial distance between two sets of points and for this manuscript the mean Hausdorff distance is utilized [34]. To compute the mean Hausdorff distance the edge of the two contours that are to be compared must be discretized into individual points.To calculate the mean Hausdorff distance one measures the distance from each point on contour A to the closest point on contour B and then averages all of these distances.

$$DSC = \frac{2X \cap Y}{X + Y}$$

i. ***Baseline performance:*** The baseline performance of each atlas to segment patients with the same scan type and vendor as those used in the atlas itself was established (Figure 1A). Atlas performance was evaluated by calculation of both DSC and Hausdorff distance metrics between manually drawn and automatic contours (via the atlas) for the three volumes of interest (VOIs): prostate, PZ and TZ.

ii. ***Contrast neutrality:*** The goal is to compare the performance of atlases, αGE_T2 and aGE_T2FS, based on differing sequences GE_T2FS and GE_ T2 sequences, respectively (comparisons shown in Figure 1B).

iii. ***Vendor neutrality:*** T2FS studies, acquired on GE and Siemens were compared (Figure 1C).

iv. ***Combined atlas:*** Determining the robustness of the segmentation when using an atlas comprising of subjects from a differing sequences or a combined atlas including subjects from both MRI vendors. The combined atlases aContrast(combined) and aVendor(combined) were compared (Figure 1D).

Atlas Generation:

A commercially available software, MIM_Maestro_v6 (MIM Software Inc, Cleveland, OH, USA) was used to build the individual vendor/contrast MRI atlases. Prostate and PZ were outlined by an expert radiation oncologist on three sets of images: GE T2, GE T2FS and Siem_T2FS. TZ volume was created by performing a Boolean operation on the Prostate and PZ. For each atlas (aGE_T2, aGE_T2FS and aSiem_T2FS) a subject free of artifact and normal positioning was selected as a template subject to which all other atlas subjects were aligned. The full pelvic MRI for each atlas subject with manually defined prostate, PZ, and TZ contours was automatically rigidly aligned to the template and added to the atlas. The combined atlases, aContrast(combined) and aVendor(combined) were created by union of the individual atlases.

Atlas Segmentation:

The atlas-based segmentation utilized the deformable image registration functionality of MIM. A leave one out approach was implemented where the target subject is removed from the atlas prior to segmentation. A schematic which demonstrates the different steps of this workflow is shown in Figure 2. The segmentation begins with aligning the patient scan to the template using rigid a transformation, based on maximizing normalized mutual information. The nine most similar atlas subjects are registered to the test case using a normalized intensity-based-free-form deformable algorithm [35,36] (Figure 2, second panel). The VOIs are then transformed to the test case utilizing this deformable registration (Figure 2, third panel) and combined using Simultaneous Truth and Performance Level Estimation (STAPLE) methods ‘ (Figure 2, fourth panel). STAPLE considers the original contours and computes a probabilistic estimate of the true representation of their combination. A measure of the positive effect each contour would have on the result is also estimated. The estimate of the “true representation” is formed by optimally combining the existing contours with weight given to their expected positive effect[37].

Comparative Analysis:

As specified above, the similarity metrics: DSC [31] and Hausdorff distance [32] were used to evaluate the atlas segmented contours in the comparisons ***(i-iv)*** for the VOIs. The DSC/

Hausdorff distance between the single expert manual contours on +/−FS is confounded by intra-reader variability and image-contrast effects. Thus the “true” similarity metrics stemming from intra-reader variability are higher than the metrics, reported by this analysis. As a measure of inter-reader variability, the volumes were contoured on GET2FS by a second expert radiation oncologist, 10 years of experience. The similarity metrics between intra- and inter-reader contours are used as benchmarks for the atlas performance. Analyses were carried out to see if these metrics differ in three sections of the prostate: base, mid and apex. These three sections of the prostate were generated by dividing the prostate into three equal parts along the Superior/Inferior axis. Similarly, the aGE_T2 and aGE_T2FS atlases were tested for variability in these sections.

To infer the variability in the atlas performances, the contrast characteristics within and surrounding the prostate were investigated. Two rind contours were created using the manually delineated prostate contour on both the T2 and T2FS scans from both vendors as shown on Supporting Figure S1. This was accomplished by expanding the prostate contour by 3mm to make an outer rind and shrinking the prostate contour by 3mm to create the inner rind. Contrast ratios between the two rinds, presented as the ratio of the means from the image intensities in both contours were estimated for T2 and T2FS scans, see equation below. Additionally, the contrast characteristics separating the TZ and PZ was also investigated by utilizing the manually delineated TZ and PZ contours for both the T2 and T2FS scans from both vendors and measuring contrast ratios between these structures to determine if atlas performance was related to contrast separation (Supporting Figure S1).

$$Contrast\ \text{Ratio} = \frac{Mean\ Signal\ \text{Intensity of Inner Rind}}{Mean\ \text{Signal Intensity of Outer Rind}}$$

RESULTS

Intra- and Inter-Reader Reproducibility of Manual Prostate and Prostate Zones Contours

The results from the comparisons of the physician drawn VOIs on T2 and T2FS are shown in Supporting Table S2. The prostate volumes on GET2FS were consistently, albeit nominally, larger than the prostate volumes on GE T2, which resulted in significant difference in the following volumes; prostate, TZ, mid-gland area of the prostate and apex area of the prostate. No significant differences in volumes were detected in either the PZ or the base region of the prostate. The manual prostate VOI demonstrates excellent reproducibility with DSC results of 0.94 and average Hausdorff Distance <1.0 mm. As expected, the PZ comparisons resulted in higher variability: DSC/Hausdorff Distance = 0.78/1.3. Also shown in Supporting Table S2 was the reproducibility of the prostate contour between the two sequences in three sections of the prostate. Again, the volumes on GE T2FS were larger than on GE T2. The contours in the base were less reproducible relative to the other two sections. The results from the inter-reader study are summarized in Supporting Table S3. There was no differences in the volumes of the contoured structures. The average DSC of 0.88 between the readers was in good agreement with previously published studies [15]. This DSC serves as a reference point for comparisons of the automatic segmentation results, as described in Figure 1.

Atlas Baseline Performance

The results from the performance of the three atlases (aGE_T2, aGE_T2FS and aSiem_T2FS, Figure 1A) when considering image, native to the particular atlas, are summarized in Table 1. Overall, the three atlases performed well for the prostate volume, with DSC results ranging from 0.79–0.83. Note that these results are within 15% of the ideal case of comparing manual contours from a single expert or intra-observer reliability (DSC=0.94, Supporting Table S2) and within 10% from the agreement between two experts or inter-observer reliability (DSC=0.88, Supporting Table S3). DSC were lower for PZ and TZ, ranging from 0.54–0.57 and 0.70–0.75, respectively. While aGE_T2FS outperformed aGE_T2, there was no significance in the metrics. aGE_T2FS also outperformed aSiem_T2FS with only one of nine measurements reaching significance, Table 2, the GE T2FS atlas significantly outperformed the Siemens_T2FS atlas using the Hausdorff metric when segmenting the transition zone. These comparisons will serve as benchmark for the subsequent analysis and referred to as ***baseline performance.***

The performance metrics were evaluated in three different sectors of the prostate. The mid-gland sector performed the best with DSC results ranging from 0.87–0.90; while the lowest DSC results originated from the base ranging from 0.68–0.76. In all sectors analyzed, the results were superior for aGE_T2FS, although there was no significance between aGE_T2FS and aSiem_T2FS, Table 2. Next, the contrast between the area immediately inside and outside the prostate and between PZ and TZ was estimated for each patient on GE T2 and GE T2FS (Supporting Table S4). GE T2 scans showed minimal differences between inside and outside the prostate, while FS scans showed on average 36% increased contrast between the rinds. FS scans demonstrated also significant contrast increase between PZ and TZ, 1.27 contrast ratio for GE T2FS scans as compared to a 1.12 contrast ratio for GE T2 scans. In all four contrast comparisons were made and all achieved significance.

Contrast Neutrality

The performance of an atlas, generated by contoured images on T2 scans (Figure 1B), in segmenting T2FS sequence and vice versa is summarized in Table 3. The aGE_T2 and aGE_T2FS performance on the differing sequence type was underwhelming with DSC results ranging from 0.09 – 0.38. The performance of the atlas aContrast(combined), however, was within the ranges of the baseline measurements in the previous section. Upon further investigation, it was determined that there was a strong trend of finding matches from the same sequence type in the combined atlas: 264/270 or 98% from T2 images and 254/270, or 90% from the T2 FS images matched images from the same sequence in the combined atlas.

Vendor Dependence

The performance of an atlas, generated by contoured images on GE T2FS in segmenting T2FS sequence on Siemens and vice versa (Figure 1C) is summarized in Table 4. The aGE_T2FS and aSiemens_T2FS performance on the differing MRI vendor were lower than the native-image comparisons, but markedly higher than the sequence neutrality results (DSC ranging from 0.43– 0.58). Again, the performance of the combined vendor atlas aVendor(combined) (Figure 1D), was higher, reaching DSC/Hausdorff Distance measures similar to the baseline measurements. Again, this was due to the fact, that 97% of GE scans were matching with GE atlas subjects and 100% of Siemens scans were matching with Siemens atlas subjects.

DISCUSSION:

The implemented method uses multi-atlas-based segmentation and as shown in Rohlfing[40] the multi-atlas-based segmentation is more successful than using a single or average atlas image. An advantage of the atlas approach is that it can be easily scaled up utilizing the MIM platform which has access to thousands of contours, generated for radiotherapy of prostate cancer. The existing workflow will allow for constant enrichment of the multi-atlas method with new cases. The novel implementation, optimized and streamlined in a commercial imaging platform resulted in fully automatic and fast (on average less than 90 sec per patient) implementation. The procedure utilizes a large array of existing robust utilities in MIM for image normalization and deformable fusion. The segmentation results (DSC of 0.83) are comparable to previously reported in atlas-based approaches: DSC of 0.85 in Klein[15]; 0.82 in Chilali[21]; 0.87 in Cheng[19]; 0.87 in Xie[18]; 0.83 in Tian[28]; and 0.87–0.88 in Korsager[20]. Note, DSC=0.83 in this work is calculated over the entire prostate, while some of the referenced studies, e.g. Cheng[19] report results in a 2D slice. As demonstrated in this report, DSC varies in the different regions of the prostate. In such cases the mid gland DSC of 0.90, as reported here, should be compared to other studies. In addition, Chilali[21] also report similar DSC for TZ (= 0.70) and PZ (= 0.62) segmentations.

As expected, the atlas more accurately segmented the prostate as compared to the PZ and the atlas performed slightly better in the mid-gland area of the prostate as compared to the base and apex. The atlas demonstrated more accurate results when segmenting the prostate contour on T2FS images as compared to T2 images, likely due to a superior contrast separation between the prostate vs the surrounding tissue. The investigation of the image-contrast impact to the atlas segmentation accuracy is novel and provides important insights. Interestingly, the decreased accuracy in zonal segmentation compared to whole prostate cannot be explained by the differences in contrast, as suggested in Chilali[21]: the contrast between PZ and TZ was similar to the contrast of the prostate and its surrounding. Similarly, for the FS data, the gains in PZ/TZ contrast did not translate in better atlas performance, indicating that there are other factors at play beyond the image contrast. In part, due to the irregular shape and relative small volume of the PZ small contouring differences can result in a large decrease in the similarity metrics. On another hand, the performance of the atlas was affected more by the contrast than the vendor. Another interesting result is that manual contours of images with lower contrast seem to underestimate the volumes.

The study has several limitations. Atlases were generated using manual segmentation performed by a single experienced operator. The intra- and inter- reader variability in contouring the prostate is well-recognized challenge [41,42] A mitigating factor is that because of the superior contrast of soft tissues on MRI, the inter-reader variability is reduced relative to other image modalities [43,44] The limited inter-reader study reported here yielded similar results to previously studies[15]. Another limitation of the work is that different subjects were used for the GE and Siemens atlases. While this hinders the direct comparison between vendors, the main finding that the target scan almost exclusively is matched by scans from the same vendor still holds.

There are a plethora of factors that affect the process of prostate segmentation: the large anatomical variability between subjects, differences in rectum and bladder filling, as well as variability in imaging data, acquired with different sequences, resolution, magnetic field, etc. The findings here show that a large multi-atlas database containing different contrast types from multiple vendors has a similar performance by forcing the target scan to match with atlas scans of the same contrast and vendor. Retrieving the relevant information from the DICOM header of the test scan to create a customized subset of atlases matched by contrast, vendor, field strength, etc. will result in efficient and fast segmentation. Future implementation of this functionality into a commercial platform will allow for universal utilization.

CONCLUSIONS:

The MRI atlas-based segmentation method achieved good results for both the whole prostate, PZ and TZ compared to expert contoured VOIs. The robustness of the proposed segmentation methods are demonstrated by utilization of combined atlases that perform similarly to matching atlas and scan type. The technique is fast, fully automatic and implemented on commercially available clinical imaging platform.

Supplementary Material

Refer to Web version on PubMed Central for supplementary material.

Acknowledgements:

This work was supported by National Cancer Institute [R01CA189295 and R01CA190105 to A.P.]. We would also like to thank Randi Steinhagen and Dr. rer. nat. Dipl.-Phys. Ellen Ackerstaff for translating our abstract into German.

REFERENCES:

1. 1Barentsz JO, Richenberg J, Clements R, et al. ESUR prostate MR guidelines 2012. Eur Radiol 2012;22:746–57. [PubMed: 22322308]
2. Weinreb JC, Barentsz JO, Choyke PL, et al. PI-RADS Prostate Imaging - Reporting and Data System: 2015, Version 2. Eur Urol 2016;69:16–40. [PubMed: 26427566]
3. Stoyanova R, Takhar M, Tschudi Y, et al. Prostate cancer radiomics and the promise of radiogenomics. Transl Cancer Res 2016;5:432–47. [PubMed: 29188191]
4. Rastinehad AR, Turkbey B, Salami SS, et al. Improving detection of clinically significant prostate cancer: magnetic resonance imaging/transrectal ultrasound fusion guided prostate biopsy. J Urol 2014;191:1749–54. [PubMed: 24333515]
5. Wysock JS, Rosenkrantz AB, Huang WC, et al. A prospective, blinded comparison of magnetic resonance (MR) imaging-ultrasound fusion and visual estimation in the performance of MR-targeted prostate biopsy: the PROFUS trial. Eur Urol 2014;66:343–51. [PubMed: 24262102]
6. of prostate segmentation algorithms for MRI: The PROMISE12 challenge. Medical Image Analysis 2014;18:359–73. [PubMed: 24418598]
7. Ou YD J; Erus G; Davatzikos C Multi_Atlas segmentation of the prostate; a zooming process with robust registration and Atlas selection. MICCAI Grand Challenge: Prostate MR Image Segmentation 2012 2012.

8. Ou Y, Sotiras A, Paragios N, Davatzikos C. DRAMMS: Deformable registration via attribute matching and mutual-saliency weighting. Med Image Anal 2011;15:622–39. [PubMed: 20688559]
9. Klein S, van der Heide UA, Haffner MC, Mosbruger T, Esopi DM, et al. Tracking the clonal origin of lethal prostate cancer. J Clin Invest 2013;123:4918–22. [PubMed: 24135135]
10. Lips IM, van der Heide UA, Haustermans K, et al. Single blind randomized phase III trial to investigate the benefit of a focal lesion ablative microboost in prostate cancer (FLAME-trial): study protocol for a randomized controlled trial. Trials 2011;12:255. [PubMed: 22141598]
11. Bauman G, Haider M, Van der Heide UA, Menard C. Boosting imaging defined dominant prostatic tumors: a systematic review. Radiother Oncol 2013;107:274–81. [PubMed: 23791306]
12. Hocht S, Aebersold DM, Albrecht C, et al. Hypofractionated radiotherapy for localized prostate cancer. Strahlenther Onkol 2017;193:1–12. [PubMed: 27628966]
13. Pathmanathan AU, van As NJ, Kerkmeijer LGW, et al. Magnetic Resonance Imaging- Guided Adaptive Radiation Therapy: A “Game Changer” for Prostate Treatment? Int J Radiat Oncol Biol Phys 2018;100:361–73. [PubMed: 29353654]
14. Hild S, Graeff C, Rucinski A, et al. Scanned ion beam therapy for prostate carcinoma: Comparison of single plan treatment and daily plan-adapted treatment. Strahlenther Onkol 2016;192:118–26. [PubMed: 26614393]
15. Litjens G, Toth R, van de Ven W, et al. Evaluation Lips IM, van Vulpen M, Staring M, Pluim JPW. Automatic segmentation of the prostate in 3D MR images by atlas matching using localized mutual information. Med Phys 2008;35:1407–17. [PubMed: 18491536]
16. Hegde JV, Mulkern RV, Panych LP, et al. Multiparametric MRI of prostate cancer: an update on state-of-the-art techniques and their performance in detecting and localizing prostate cancer. J Magn Reson Imaging 2013;37:1035–54. [PubMed: 23606141]
17. Bhavsar A, Verma S. Anatomic imaging of the prostate. Biomed Res Int 2014;2014:728539. [PubMed: 25243174]
18. Xie Q, Ruan D. Low-complexity atlas-based prostate segmentation by combining global, regional, and local metrics. Med Phys 2014;41:041909. [PubMed: 24694140]
19. Cheng R, Turkbey B, Gandler W, et al. Atlas based AAM and SVM model for fully automatic MRI prostate segmentation. Conf Proc IEEE Eng Med Biol Soc 2014;2014:2881–5.
20. Korsager AS, Fortunati V, van der Lijn F, et al. The use of atlas registration and graph cuts for prostate segmentation in magnetic resonance images. Med Phys 2015;42:1614–24. [PubMed: 25832052]
21. Chilali O, Puech P, Lakroum S, Diaf M, Mordon S, Betrouni N. Gland and Zonal Segmentation of Prostate on T2W MR Images. J Digit Imaging 2016.
22. Wu K, Garnier C, Alirezaie J, Dillenseger JL. Adaptation and evaluation of the multiple organs OSD for T2 MRI prostate segmentation. Conf Proc IEEE Eng Med Biol Soc 2014;2014:4687–90.
23. Makni N, Iancu A, Colot O, Puech P, Mordon S, Betrouni N. Zonal segmentation of prostate using multispectral magnetic resonance images. Med Phys 2011;38:6093–105. [PubMed: 22047374]
24. Litjens G, Debats O, van de Ven W, Karssemeijer N, Huisman H. A pattern recognition approach to zonal segmentation of the prostate on MRI. Med Image Comput Comput Assist Interv 2012;15:413–20. [PubMed: 23286075]
25. Maan B, van der Heijden F, Futterer JJ. A new prostate segmentation approach using multispectral Magnetic Resonance Imaging and a statistical pattern classifier. Proc Spie 2012;8314.
26. Chowdhury N, Toth R, Chappelow J, et al. Concurrent segmentation of the prostate on MRI and CT via linked statistical shape models for radiotherapy planning. Med Phys 2012;39:2214–28. [PubMed: 22482643]
27. Toth R, Madabhushi A. Multifeature landmark-free active appearance models: application to prostate MRI segmentation. IEEE Trans Med Imaging 2012;31:1638–50. [PubMed: 22665505]
28. Tian Z, Liu L, Fei B. A fully automatic multi-atlas based segmentation method for prostate MR images. Proc SPIE Int Soc Opt Eng 2015;9413.
29. Rothke M, Blondin D, Schlemmer HP, Franiel T. PI-RADS Classification: Structured Reporting for MRI of the Prostate. Rofo-Fortschr Rontg 2013;185:253–61.

30. Rosenkrantz AB, Taneja SS. Radiologist, be aware: ten pitfalls that confound the interpretation of multiparametric prostate MRI. AJR Am J Roentgenol 2014;202:109–20. [PubMed: 24370135]
31. Dice LR. Measures of the Amount of Ecologic Association between Species. Ecology 1945;26:297–302.
32. Hausdorff F Grundzdge der Mengenlehre. Leipzig: Veit; 1914.
33. Zou KH, Warfield SK, Bharatha A, et al. Statistical validation of image segmentation quality based on a spatial overlap index. Acad Radiol 2004;11:178–89. [PubMed: 14974593]
34. Huttenlocher DP, Klanderman GA, Rucklidge WJ. Comparing Images Using the Hausdorff Distance. Ieee T Pattern Anal 1993;15:850–63.
35. Piper JN A; Harper J Deformable Image Registration in MIM Maestro Evaluation and Description. Company White Paper 2013:5.
36. Johnson PB, Padgett KR, Chen KL, Dogan N. Evaluation of the tool "Reg Refine" for user- guided deformable image registration. J Appl Clin Med Phys 2016;17:158–70.
37. Warfield SK, Zou KH, Wells WM. Simultaneous truth and performance level estimation (STAPLE): an algorithm for the validation of image segmentation. IEEE Trans Med Imaging 2004;23:903–21. [PubMed: 15250643]
38. Hoeks CMA, Barentsz JO, Hambrock T, et al. Prostate Cancer: Multiparametric MR Imaging for Detection, Localization, and Staging. Radiology 2011;261:46–66. [PubMed: 21931141]
39. McGurk RJ, Bowsher J, Lee JA, Das SK. Combining multiple FDG-PET radiotherapy target segmentation methods to reduce the effect of variable performance of individual segmentation methods. Med Phys 2013;40:042501. [PubMed: 23556917]
40. Rohlfing T, Brandt R, Menzel R, Maurer CR, Jr. Evaluation of atlas selection strategies for atlas-based image segmentation with application to confocal microscopy images of bee brains. Neuroimage 2004;21:1428–42. [PubMed: 15050568]
41. Fiorino C, Reni M, Bolognesi A, Cattaneo GM, Calandrino R. Intra- and inter-observer variability in contouring prostate and seminal vesicles: implications for conformal treatment planning. Radiother Oncol 1998;47:285–92. [PubMed: 9681892]
42. Choi HJ, Kim YS, Lee SH, et al. Inter- and intra-observer variability in contouring of the prostate gland on planning computed tomography and cone beam computed tomography. Acta Oncol 2011;50:539–46. [PubMed: 21391773]
43. Lutgendorf-Caucig C, Fotina I, Stock M, Potter R, Goldner G, Georg D. Feasibility of CBCT-based target and normal structure delineation in prostate cancer radiotherapy: multi-observer and image multi-modality study. Radiother Oncol 2011;98:154–61. [PubMed: 21176984]
44. Villeirs GM, Van Vaerenbergh K, Vakaet L, et al. Interobserver delineation variation using CT versus combined CT + MRI in intensity-modulated radiotherapy for prostate cancer. Strahlenther Onkol 2005;181:424–30. [PubMed: 15995835]

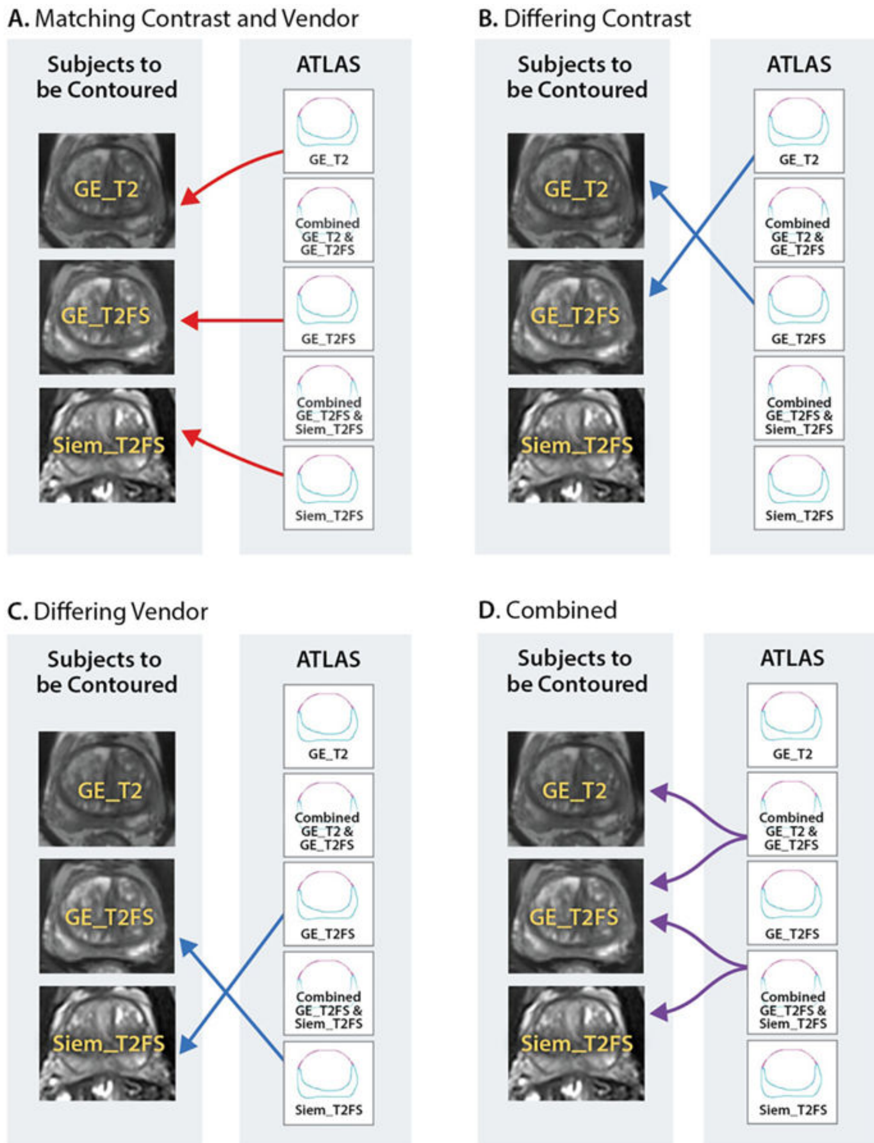

Figure 1:

The performance of five atlases was evaluated. Each atlas was created by combining imaging data from all or subset of three sets of data: GE_T2 and GE_T2FS and Siem_T2FS. **A:** Baseline performance: Matching contrast and vendor - Three atlases: αGE_T2, αGE_T2FS and αSiem_T2FS were generated from each dataset and the auto-segmentation evaluated on the native images for each atlas; **B:** Differing contrast: The auto-segmentation was evaluated on +/− FS images; **C:** Differing Vendor: The auto-segmentation is evaluated on the images from different vendor; **D:** Combined atlases: αContrast(combined) and aVendor(combined) are evaluated on each dataset.

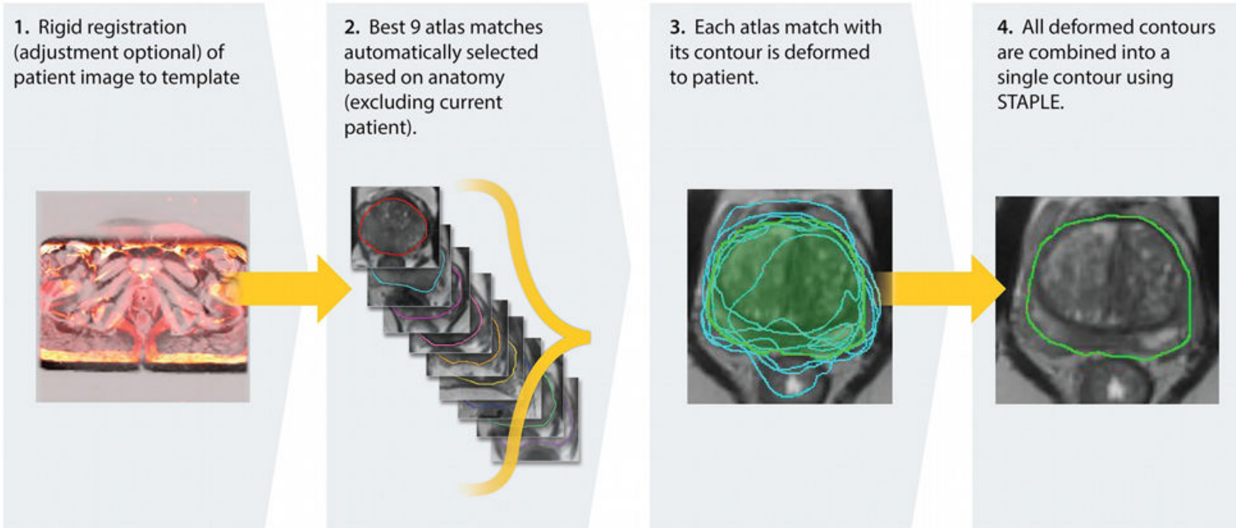

Figure 2:

Schema of atlas segmentation workflow.

Table 1:

MRI acquisition parameters*.

Axial Sequence	TR/TE (msec)	Slice thickness (mm)	# of slices	Matrix	FOV (mm)	Voxel size (mm)	Total scan time(sec)
GE_T2	5420/101	2.5	72	256 ×256	320 × 320	1.25 × 1.25	347
GE_T2FS	5565/101	2.5	72	256×256	320 × 320	1.25 × 1.25	356
Siem_T2FS	6300/112	2.5	72	256 × 192	360 × 270	1.41 × 1.41	302

Abbreviations: FOV = Field of View; FS = Fat Saturated; TE = Echo Time; TR = Repetition Time.

*MRI data were acquired in part for the purposes of radiotherapy planning, including a fusion with CT. The high spatial resolution and full pelvis coverage enables accurate registration between MRI and CT.

Table 2:

Similarity metrics (Dice Similarity Coefficient; Hausdorff Distance) for Prostate, Peripheral Zone, and Transition Zone between manual and automatic contours. Below: Similarity metrics for prostate, calculated separately for the three sections of the gland.

Volume of Interest	Matching Atlas and Scan Type	Dice Similarity Coefficient (mean±σ)	Hausdorff Distance (mm) (mean±σ)
Prostate	αGE_T2	0.81 ±0.15	2.7 ± 1.9
	αGE_T2FS	0.83 ±0.06	2.4 ±0.8
	αSiem_T2FS	0.79 ±0.14	2.9 ± 1.6
Peripheral Zone	αGE_T2	0.60 ±0.17	2.7 ± 1.4
	αGE_T2FS	0.59 ± 0.13	2.7 ± 1.0
	αSiem T2FS	0.54 ± 0.16	3.1 ± 1.5
Transition Zone	αGE_T2	0.74 ±0.17	3.1 ±2.2
	αGE_T2FS	0.75 ±0.09	2.9 ±0.9
	αSiem T2FS	0.70 ±0.14	3.6* ± 1.4
Base	αGE_T2	0.76 ±0.19	3.8 ±4.6
	αGE_T2FS	0.73 ±0.08	3.5 ± 1.2
	αSiem_T2FS	0.68 ±0.16	4.0 ± 1.8
Mid Gland	αGE_T2	0.87 ± 0.14	2.2 ± 1.9
	αGE_T2FS	0.90 ±0.05	1.8 ± 0.9
	αSiem T2FS	0.87 ± 0.15	2.2 ± 1.9
Apex	αGE_T2	0.79 ± 0.15	2.2 ± 1.3
	αGE_T2FS	0.83 ±0.07	1.9 ± 0.6
	αSiem_T2FS	0.79 ±0.16	2.0 ±0.9

*Significantly different from aGE_T2FS, based on two-tailed Student's t-test, p-value < 0.05.

Table 3:

Summary of contrast neutrality results. For the whole prostate and the zonal anatomy the performance of the differing contrast type (i.e. a T2 scan using the T2FS atlas and vice versa) atlas is shown. The results of the combined contrast atlas: aContrast(combined)=aGE_T2 U aGE T2FS are also shown.

Volume of Interest	Scan Type	Atlas	Dice Similarity Coefficient	Hausdorff Distance (mm)
Whole Prostate	GE_T2	αGE_T2FS	0.25 ± 0.28	8.6 ± 14.6
	GE_T2FS	αGE_T2	0.38 ±0.32	13.5 ±25.9
	GE_T2	αContrast(combined)	0.76 ±0.15	2.6 ± 1.8
	GE_2FS	αContrast(combined)	0.80 ±0.08	2.3 ±0.9
Peripheral Zone	GE_T2	αGE_T2FS	0.19 ±0.21	7.7 ± 13.8
	GE_T2FS	αGE_T2	0.09 ±0.13	9.6 ± 17.7
	GE_T2	αContrast(combined)	0.49 ±0.14	2.7 ± 1.3
	GE_T2FS	αContrast(combined)	0.59 ±0.13	2.4 ± 1.0
Transition Zone	GE_T2	αGE_T2FS	0.32 ±0.29	14.3 ±25.8
	GE_T2FS	αGE_T2	0.22 ± 0.27	8.5 ± 15.6
	GE_T2	αContrast(combined)	0.68 ±0.17	3.0 ± 2.0
	GE_T2FS	αContrast(combined)	0.72 ±0.17	2.5 ±0.9

Table 4:

Summary of vendor neutrality results. For the whole prostate and the zonal anatomy the performance of the opposing MRI vendor (i.e. a GET2FS scan using the αSiem_T2FS) atlas is shown. The results of combined vendor atlas αVendor(combined)=αGE_T2FS El αSiem_T2FS are also shown.

Volume of Interest	Type	Atlas	Dice Similarity Coefficient	Hausdorff Distance (mm)
Prostate	GE_T2FS	αSiem_T2FS	0.58 ±0.26	8.4 ± 15.3
	Siem_T2FS	αGE_T2FS	0.43 ±0.31	12.2 ± 13.0
	GE_T2FS	αV endor(combined)	0.82 ±0.08	2.2 ± 1.7
	Siem_T2FS	αV endor(combined)	0.79 ±0.14	2.4 ± 1.5
Peripheral Zone	GE_T2FS	αSiem_T2FS	0.32 ±0.24	11.1 ± 18.4
	Siem_T2FS	αGE_T2FS	0.25 ± 0.24	13.2 ± 15.0
	GE_T2FS	αV endor(combined)	0.57 ±0.15	2.4 ± 1.3
	Siem_T2FS	αV endor(combined)	0.52 ±0.19	2.7 ±2.0
Transition Zone	GE_T2FS	αSiemens_T2FS	0.52 ±0.26	8.5 ± 15.2
	Siem_T2FS	αGE_T2FS	0.33 ±0.27	12.6 ± 13.6
	GE_T2FS	αV endor(combined)	0.73 ±0.16	3.0 ± 4.6
	Siem_T2FS	αVendor(combined)	0.71 ±0.14	2.7 ± 1.5